Astroglial networks scale synaptic activity and plasticity

Ulrike Pannasch[a], Lydia Vargová[b,c], Jürgen Reingruber[d], Pascal Ezan[a], David Holcman[d], Christian Giaume[a], Eva Syková[b,c], and Nathalie Rouach[a,1]

[a]Center for Interdisciplinary Research in Biology, Centre National de la Recherche Scientifique Unité Mixte de Recherche 7241/Institut National de la Santé et de la Recherche Médicale U1050, Collège de France, 75005 Paris, France; [b]Department of Neuroscience and Center for Cell therapy and Tissue Repair, Charles University, Second Faculty of Medicine, 150 06 Prague, Czech Republic; [c]Department of Neuroscience, Institute of Experimental Medicine of the Academy of Sciences of the Czech Republic, 142 20 Prague, Czech Republic; and [d]Institut de Biologie de l'Ecole Normale Supérieure, Centre National de la Recherche Scientifique Unité Mixte de Recherche 8197/Institut National de la Santé et de la Recherche Médicale U1024, Department of Computational Biology and Mathematics, Ecole Normale Supérieure, Paris, 75005, France

Edited* by Roger A. Nicoll, University of California, San Francisco, CA, and approved April 11, 2011 (received for review November 22, 2010)

Astrocytes dynamically interact with neurons to regulate synaptic transmission. Although the gap junction proteins connexin 30 (Cx30) and connexin 43 (Cx43) mediate the extensive network organization of astrocytes, their role in synaptic physiology is unknown. Here we show, by inactivating Cx30 and Cx43 genes, that astroglial networks tone down hippocampal synaptic transmission in CA1 pyramidal neurons. Gap junctional networking facilitates extracellular glutamate and potassium removal during synaptic activity through modulation of astroglial clearance rate and extracellular space volume. This regulation limits neuronal excitability, release probability, and insertion of postsynaptic AMPA receptors, silencing synapses. By controlling synaptic strength, connexins play an important role in synaptic plasticity. Altogether, these results establish connexins as critical proteins for extracellular homeostasis, important for the formation of functional synapses.

hippocampus | neuroglial interactions

Astrocytes, elements of the tripartite synapse, integrate and modulate neuronal excitability, synaptic transmission, and plasticity (1). Up to now the involvement of astrocytes in central functions has mostly been considered to result from the activity of individual astrocytes. However, a typical feature of astrocytes is their network organization provided by numerous gap junction channels formed by two main connexin (Cx) subunits, Cx43, present from embryonic to adult stages, and Cx30, expressed later in development (2). Gap junction channels consist of two hemichannels, each composed of six Cx subunits that align between adjacent cells to form intercellular channels. They mediate direct intercellular communication involving exchange of ions (electrical coupling) and small signaling molecules (biochemical coupling), with a molecular weight up to 1.5 kDa. Intercellular trafficking and redistribution of neuroactive substances, such as ions and neurotransmitters, through gap junction channels during neuronal activity suggest that astroglial network communication plays a role in neuroglial interactions and neurotransmission. This hypothesis is supported by altered behavior in Cx30 and astrocyte-targeted Cx43 knockout mice (3), as well as by impairment in sensorimotor and spatial memory tasks in Cx43 and Cx30 double-knockout mice (4). In addition, these channels have recently been shown to be important for neuronal activity during pathological conditions, such as hypoglycemia (5) and epilepsy (6), by mediating nutrient transport and spatial potassium buffering, respectively. However, their role in basal neurotransmission and synaptic plasticity is unknown. Thus, the aim of this work was to determine whether and how the connectivity of astroglial networks contributes to basal synaptic transmission and plasticity. We here demonstrate that mice deficient for both astroglial Cx30 and Cx43 have increased hippocampal synaptic transmission and impaired long-term synaptic plasticity. These effects are due to decreased astroglial glutamate and potassium clearance and altered extracellular space volume regulation during synaptic activity. This impairment results in increased neuronal excitability, release probability, glutamate spillover, and insertion of postsynaptic AMPARs, unsilencing synapses. Altogether, our findings indicate that gap junction-mediated astroglial networks control synaptic strength by modulating extracellular homeostasis.

Results

To examine the role of astroglial connexins in hippocampal neurotransmission, we used the double-knockout mice for Cx30 and Cx43 ($Cx30^{-/-}Cx43^{-/-}$), in which gap junctional communication is totally disrupted, as shown by dye coupling experiments ($Cx30^{-/-}Cx43^{-/-}$, 0 ± 0 coupled cells, n = 18 vs. WT, 36 ± 6 coupled cells, n = 21; Fig. S1 *A* and *B*). Hippocampi from $Cx30^{-/-}Cx43^{-/-}$ mice (P16–25) exhibit normal architecture and layered structure (Fig. 1*A*). CA1 vacuolation, previously described in older mice (P23–adult) (4), was not observed. In addition, we found comparable densities of CA1 pyramidal neurons (NeuN positive) and astrocytes (S100 positive) (Fig. 1*B*), as recently shown in older $Cx30^{-/-}Cx43^{-/-}$ mice (4), although a reduced number of radial glia-like cells and granule neurons was reported in the dentate gyrus (7). Western blot analysis for the pre- and postsynaptic proteins synaptophysin and PSD-95, respectively, revealed no difference between wild type and $Cx30^{-/-}Cx43^{-/-}$ mice, suggesting similar total synaptic contacts (Fig. 1*C*).

To study excitatory synaptic transmission at CA1 Schaffer collateral synapses, we evoked AMPAR-mediated field excitatory postsynaptic potentials (fEPSPs) in acute hippocampal slices, where the size of the presynaptic fiber volley (input) was compared with the slope of the fEPSP (output), and found a 100% increase in synaptic transmission in $Cx30^{-/-}Cx43^{-/-}$ mice ($P < 0.05$, n = 19) relative to wild-type animals (n = 23, Fig. 1*D*). In addition to the important increase in excitatory postsynaptic currents (EPSCs) ($P < 0.001$, EPSC amplitude, $Cx30^{-/-}Cx43^{-/-}$, −114 ± 5 pA, n = 5 vs. WT, −51 ± 5 pA, n = 5; Fig. 1*E*), whole-cell voltage clamp experiments also revealed an increase in inhibitory postsynaptic currents (IPSCs) in CA1 pyramidal neurons from $Cx30^{-/-}Cx43^{-/-}$ mice ($P < 0.001$, IPSC amplitude, $Cx30^{-/-}Cx43^{-/-}$, 241 ± 19 pA, n = 5 vs. WT, 83 ± 13 pA, n = 5; Fig. 1*E*), indicating a general augmentation in synaptic transmission.

Author contributions: U.P., L.V., E.S., and N.R. designed research; U.P., L.V., P.E., and N.R. performed research; C.G. contributed new reagents/analytic tools; U.P., L.V., J.R., D.H., and N.R. analyzed data; and U.P., L.V., D.H., and N.R. wrote the paper.

The authors declare no conflict of interest.

*This Direct Submission article had a prearranged editor.

[1]To whom correspondence should be addressed. E-mail: nathalie.rouach@college-de-france.fr.

This article contains supporting information online at www.pnas.org/lookup/suppl/doi:10.1073/pnas.1016650108/-/DCSupplemental.

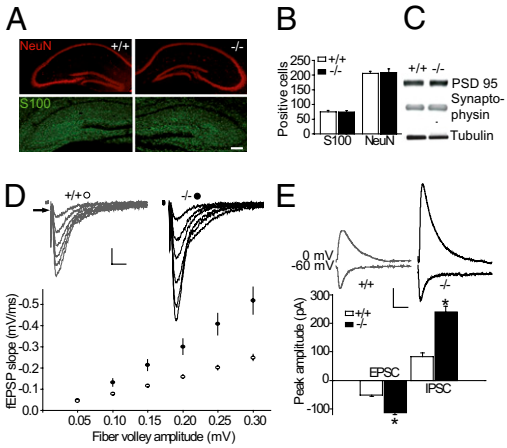

Fig. 1. Synaptic transmission of CA1 pyramidal cells is increased in Cx30$^{-/-}$Cx43$^{-/-}$ mice. (*A*) Normal hippocampal morphology was revealed in Cx30$^{-/-}$Cx43$^{-/-}$ hippocampal slices by immunostaining with the neuronal marker NeuN and the astrocyte marker S100. (Scale bar, 200 μm.) (*B*) Quantification of NeuN (Cx30$^{-/-}$Cx43$^{-/-}$, n = 7; WT, n = 7) and S100 positive cells (Cx30$^{-/-}$Cx43$^{-/-}$, n = 8; WT, n = 8,) revealed no difference in cell numbers. (*C*) Levels of pre- and postsynaptic markers, synaptophysin and PSD-95, respectively, are similar in Cx30$^{-/-}$Cx43$^{-/-}$ and wild-type mice. Similar tubulin (Tub) levels confirm equivalent loading. (*D*) Basal excitatory transmission is enhanced in Cx30$^{-/-}$Cx43$^{-/-}$ hippocampal slices (P < 0.05, n = 20), as assessed by input–output curves. As illustrated in the sample traces and the graph below, for each input (fiber volley, see arrow), the output (fEPSP) is increased compared with that in wild-type mice (n = 23). (Scale bar, 0.2 mV, 10 ms.) (*E*) Inhibitory transmission is also enhanced in CA1 pyramidal cells from Cx30$^{-/-}$Cx43$^{-/-}$ mice (n = 5), as revealed by recordings of EPSCs (at −60 mV) and IPSCs (at 0 mV, P < 0.0001) in the same pyramidal cell (WT, n = 5). (Scale bar, 50 pA, 50 ms.)

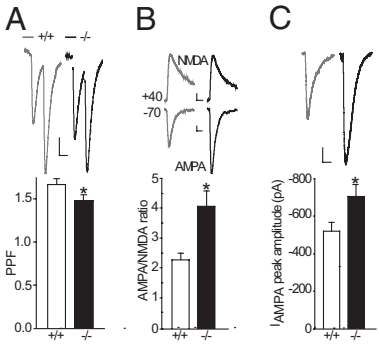

Fig. 2. Pre- and postsynaptic properties are altered in pyramidal cells from Cx30$^{-/-}$Cx43$^{-/-}$ mice. (*A*) Release probability is increased in Cx30$^{-/-}$Cx43$^{-/-}$ mice, as indicated by decreased paired pulse facilitation (P < 0.05, Cx30$^{-/-}$Cx43$^{-/-}$, n = 15; WT, n = 18). Representative EPSC traces are shown above the bar graph. (Scale bar, 10 pA, 25 ms.) (*B*) AMPAR activity is enhanced in Cx30$^{-/-}$Cx43$^{-/-}$ mice, as shown by increased AMPA-NMDA EPSC ratios measured in pyramidal cells (n = 17) compared with wild-type mice (n = 21, P < 0.001). (Scale bar, 5 pA, 20 ms.) (*C*) Local application of AMPA (10 μM + 0.5 μM tetrodotoxin + 100 μM cyclothiazide) induced bigger responses in CA1 pyramidal cells from Cx30$^{-/-}$Cx43$^{-/-}$ mice (P < 0.05, n = 11), compared with wild type (n = 20). (Scale bar, 100 pA, 20 s.)

What may cause increased synaptic transmission in Cx30$^{-/-}$Cx43$^{-/-}$ mice? We first determined whether intrinsic membrane properties of CA1 pyramidal cells were altered and found no difference in their resting membrane potential (V_m, Cx30$^{-/-}$Cx43$^{-/-}$, −59.7 ± 0.7 mV, n = 38 vs. WT, −59.5 ± 0.9 mV, n = 34) and membrane resistance (R_m, Cx30$^{-/-}$Cx43$^{-/-}$, 225.8 ± 14.2 MΩ, n = 38 vs. WT, 203.7 ± 16.2 MΩ, n = 34). However, excitability of pyramidal cells from Cx30$^{-/-}$Cx43$^{-/-}$ mice was increased, because they show enhanced firing rate for low depolarizing current pulses (Fig. S2 *A* and *B*). Indeed, the minimal current necessary to induce action potentials, the rheobase, was reduced by nearly 50% in pyramidal cells from Cx30$^{-/-}$Cx43$^{-/-}$ mice (P < 0.01, Cx30$^{-/-}$Cx43$^{-/-}$, 15.6 ± 2.3 pA, n = 22 vs. WT, 27.7 ± 3.8 pA, n = 18; Fig. S2*C*), whereas there was no difference in the amplitude of evoked action potentials (Fig. S2*C*). To determine whether transmitter release was increased, we recorded paired pulse facilitation (PPF), a form of short-term plasticity sensitive to changes in release probability. PPF was decreased in Cx30$^{-/-}$Cx43$^{-/-}$ mice (P < 0.05, Cx30$^{-/-}$Cx43$^{-/-}$, 1.5 ± 0.05, n = 15 vs. WT, 1.7 ± 0.06, n = 18; Fig. 2*A*), indicating an increase in the probability of presynaptic release.

Increased glutamate release should affect similarly postsynaptic AMPARs and NMDARs. However, by comparing the AMPAR and NMDAR components of the EPSC, we found that the AMPA/NMDA ratio was increased by ∼80% in pyramidal cells from Cx30$^{-/-}$Cx43$^{-/-}$ mice (P < 0.001, ratio of Cx30$^{-/-}$Cx43$^{-/-}$, 4.1 ± 0.5, n = 17; WT, 2.3 ± 0.2, n = 21; Fig. 2*B*), suggesting additional alterations in postsynaptic AMPAR density. To further examine whether the functional AMPAR membrane density is enhanced in pyramidal cells from Cx30$^{-/-}$Cx43$^{-/-}$ mice, AMPA was locally applied throughout the cells, which activates synaptic and extrasynaptic AMPARs. The amplitude of the evoked whole-cell current was increased by ∼40% in Cx30$^{-/-}$Cx43$^{-/-}$ mice (P < 0.05, Cx30$^{-/-}$Cx43$^{-/-}$, −705 ± 64 pA, n = 11; WT, −493 ± 46, n = 20; Fig. 2*C*), suggesting an overall increase in surface AMPAR density in pyramidal cells.

Because postsynaptic AMPAR trafficking is activity dependent and can unsilence synapses during development (8), the occurrence of silent synapses may be decreased in Cx30$^{-/-}$Cx43$^{-/-}$ mice. To examine this possibility, we used minimal stimulation to compare the failure rate of synaptic AMPAR responses in wild type and Cx30$^{-/-}$Cx43$^{-/-}$ mice, for similar release probabilities (Fig. 3*A*). This comparison was performed by decreasing the extracellular Ca/Mg ratio (from 2.5 mM Ca/1.3 mM Mg to 2.2 mM Ca/1.6 mM Mg) to reduce the release probability in Cx43$^{-/-}$Cx30$^{-/-}$ mice to wild-type levels, as measured by PPF (WT, 1.7 ± 0.03, n = 9; Cx30$^{-/-}$Cx43$^{-/-}$ in 2.2 mM Ca/1.6 mM Mg, 1.7 ± 0.04, n = 10; Fig. 3*B*). As shown in the superimposed recordings in Fig. 3*A*, the failure rate is reduced and the amplitude of EPSCs is increased in hippocampal cells from Cx30$^{-/-}$Cx43$^{-/-}$ mice (Fig. 3 *C* and *D*). To ensure that this result was not attributable to the pyramidal cells receiving more synaptic inputs in Cx30$^{-/-}$Cx43$^{-/-}$ mice, we compared the size of the NMDA component of the EPSC at +40 mV in both genotypes and found no difference (Cx30$^{-/-}$Cx43$^{-/-}$, 10.9 ± 2.3 pA, n = 10 vs. WT, 10.3 ± 1.5 pA, n = 9; Fig. 3*C*). These data indicate a higher number of functional synapses in Cx43$^{-/-}$Cx30$^{-/-}$ mice.

Synapse unsilencing can occur during synaptic plasticity and potentiate synaptic transmission (9). Therefore, we examined the possibility that the reduced pool of silent synapses in Cx30$^{-/-}$Cx43$^{-/-}$ mice occluded long-term potentiation (LTP). We found that LTP, recorded by field potentials and induced by brief tetanic stimulation (two 1-s trains of 100 Hz, 20 s apart) of Schaffer collaterals, was nearly absent at CA1 synapses from Cx30$^{-/-}$Cx43$^{-/-}$ mice, as LTP was decreased by ∼80% (30–40 min after the tetanus, n = 9) compared with wild-type mice (n = 9, Fig. 3*E*). We next investigated whether long-term depression (LTD) of CA1 pyramidal cells was also altered in Cx30$^{-/-}$Cx43$^{-/-}$ mice and found, using field potential recordings, an increased magnitude of LTD (∼100%) in these mice, because the fEPSP slope was decreased by ∼40% (30–40 min after LTD induction, n = 5), whereas it was reduced by only ∼20% in wild-type animals (P < 0.0001, n = 5; Fig. 3*F*). Interestingly, LTP was restored in Cx30$^{-/-}$Cx43$^{-/-}$ mice (∼58% fEPSP slope increase 30–40 min after LTP induction, n = 5; Fig. S3) when synapse depotentiation

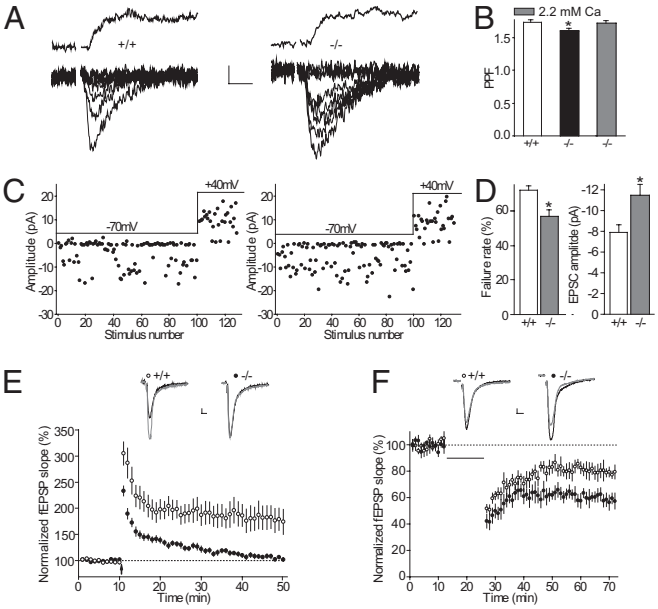

Fig. 3. Astroglial Cx43 and -30 deficiency unsilences hippocampal CA1 synapses, occludes long-term potentiation, and enhances long-term depression. (*A*) Reduction of silent synapses at hippocampal pyramidal cells from Cx30$^{-/-}$Cx43$^{-/-}$ mice, illustrated by 10 superimposed traces of response at −70 mV to minimal stimulation in neurons from wild-type and Cx30$^{-/-}$Cx43$^{-/-}$ mice. (*A*, *Upper*) Mean traces illustrate the corresponding NMDA response at +40 mV, in the presence of CNQX. (Scale bar, 5 pA, 10 ms.) (*B*) The enhanced release probability in Cx30$^{-/-}$Cx43$^{-/-}$ mice was reduced to wild-type level by lowering the extracellular Ca/Mg ratio (from 2.5 mN Ca/1.3 mM Mg to 2.2 mM Ca/1.6 mM Mg) during minimal stimulation. (*C*) Plots of EPSC amplitude versus trial number at −70 and +40 mV. (*D*) Minimal stimulation revealed less AMPAR response failures and increased EPSC amplitude in pyramidal cells from Cx30$^{-/-}$Cx43$^{-/-}$ mice ($P < 0.005$, $n = 10$) compared with wild-type mice ($n = 9$). (*E*) LTP, produced by two 100-Hz tetani separated by 20 s (arrow), was nearly absent in slices from Cx30$^{-/-}$Cx43$^{-/-}$ mice ($P < 0.005$, $n = 9$), whereas it was induced in wild-type slices ($n = 9$). (*E*, *Upper*) Representative traces of averaged fEPSP recordings in slices before (solid traces) and 40–50 min after tetanic stimulation of Schaffer collaterals (shaded traces) are shown. (Scale bar, 0.05 mV, 10 ms.) (*F*) LTD, induced by 1-Hz stimulation over 15 min, as indicated by a solid line, was increased by ∼100% in Cx30$^{-/-}$Cx43$^{-/-}$ mice ($P < 0.05$, $n = 5$), compared with wild-type mice ($n = 5$). (*F*, *Upper*) Sample traces represent averaged field potentials before (solid traces) and 50–60 min after tetanization (shaded traces). (Scale bar, 0.05 mV, 10 ms.)

by LTD induction was performed before tetanic stimulation of Schaffer collaterals to induce LTP. Altogether these findings indicate that deficiency for Cx30 and Cx43 leads to synapse unsilencing, therefore inducing profound alterations in the plasticity of pyramidal cells, favoring synaptic depression.

Which alterations in disconnected astrocytes may cause increased synaptic transmission? Astroglial whole-cell current profiles (Fig. S1 *C* and *D*), intrinsic membrane properties, resting membrane potential, and membrane resistance (Fig. S1*E*) did not differ between both genotypes. Gliotransmitter release (ATP, glutamate, and D-serine), shown to modulate synaptic transmission (1), was also unchanged in disconnected astrocytes during basal neuronal activity evoked by stimulation of the Schaffer collaterals, because blocking the targeted neuronal receptors, i.e., adenosine A1 receptors by 8-cyclopentyl-1,3-dipropylxanthine (DPCPX) and NMDARs by (RS)-3-(2-Carboxypiperazin-4-yl-)-propyl-1-phosphonic acid (RS-CPP), had no differential effect on excitatory transmission of CA1 pyramidal cells from wild-type and Cx30$^{-/-}$Cx43$^{-/-}$ mice (Fig. S4*A*). Because increased synaptic activity in Cx30$^{-/-}$Cx43$^{-/-}$ mice may result from inadequate ion/neurotransmitter uptake, we investigated the ability of disconnected astrocytes to buffer potassium and uptake glutamate released synaptically. For this purpose, we first measured simultaneously synaptically evoked glutamate transporter (GLT) or potassium (K^+) currents in astrocytes (Fig. S5 *C* and *F*, respectively) and neuronal responses (fEPSPs, Fig. S5*A*), induced in wild-type and Cx30$^{-/-}$Cx43$^{-/-}$ hippocampal slices by similar Schaffer collateral stimulation, as assessed by comparable fiber volley amplitudes from fEPSPs (for GLT currents, Cx30$^{-/-}$Cx43$^{-/-}$, −0.28 ± 0.04 mV, $n = 6$ vs. WT, −0.3 ± 0.03 mV, $n = 6$; for K^+ currents, Cx30$^{-/-}$Cx43$^{-/-}$, −0.24 ± 0.03 mV, $n = 9$ vs. WT, −0.29 ± 0.02 mV, $n = 7$). Peak amplitudes of evoked astroglial GLT and K^+ currents, isolated pharmacologically (Fig. S5 *B* and *C* and *E* and *F*, respectively), were increased by ∼86% ($n = 6$) and ∼79% ($n = 9$), respectively, in Cx30$^{-/-}$Cx43$^{-/-}$ mice relative to wild-type animals ($n = 7$ and $n = 6$, respectively; Fig. 4 *A* and *F*). The enhanced astroglial GLT and K^+ current amplitudes reflect the increased synaptic activity in Cx30$^{-/-}$Cx43$^{-/-}$ mice, because they were comparable to wild-type current amplitudes when normalized to the associated excitatory transmission (Fig. 4 *A* and *F*), calculated by the fEPSP slope/fiber volley ratio (Fig. S5 *D* and *G*). However, Cx30$^{-/-}$Cx43$^{-/-}$ astrocytes fail to properly remove the enhanced extracellular glutamate and potassium levels during synaptic activity. Indeed GLT currents exhibited slower decay kinetics in Cx30$^{-/-}$Cx43$^{-/-}$ mice (Fig. 4*B*). In addition, the actual time course of astroglial glutamate clearance, derived from the recorded GLT currents by taking into account its filtering (by factors such as electrical properties of astrocytes or asynchronous transmitter release, distorting GLT current kinetics) (10), was nearly two times slower in Cx30$^{-/-}$Cx43$^{-/-}$ mice ($P < 0.05$, Cx30$^{-/-}$Cx43$^{-/-}$, 10 ± 1.4 ms, $n = 5$; WT, 5.2 ± 0.9 ms, $n = 5$; Fig. 4*C*).

Consistent with the decreased astroglial glutamate clearance, we found that released glutamate persists longer at the synapse, because the kinetics of evoked AMPAR EPSCs, measured in the presence of cyclothiazide (100 μM) to prevent receptor desensitization and known to be altered by glial GLT inhibition (11–13), revealed prolonged decay times (∼30%) in Cx30$^{-/-}$Cx43$^{-/-}$ mice for similar current amplitudes than in wild-type mice (Cx30$^{-/-}$Cx43$^{-/-}$, −113 ± 1 pA, $n = 5$ vs. WT, −111 ± 0.7 pA, $n = 6$) (Fig. 4*D*). In addition, because astroglial GLTs limit glutamate spillover in CA1 (14), activating NMDARs (14, 15), we investigated decay kinetics of evoked NMDAR EPSCs and found that they were also prolonged (∼20%) in Cx30$^{-/-}$Cx43$^{-/-}$ mice (Fig. S6*B*). This decay prolongation was likely due to the weaker and slower activation of distant receptors on neighboring synapses, because D-alpha-amino adipate (D-AA, 70 μM), a low-affinity competitive NMDAR antagonist inhibiting mostly receptors encountering low glutamate concentration, accelerated the NMDAR EPSCs half decay times by ∼20% in Cx30$^{-/-}$Cx43$^{-/-}$ mice, whereas it had no effect in wild-type mice (Fig. 4*E*), as previously shown (15). Altogether, this result demonstrates that glutamate spillover, activating NMDARs, occurs only in Cx30$^{-/-}$Cx43$^{-/-}$ mice. Neuronal GLT EAAT3 (also known as EAAC1) and EAAT4 levels are regulated by neuronal activity (16) and also contribute to hippocampal glutamate clearance, limiting NMDAR activation by glutamate spillover (15). However, they are unlikely to contribute to the enhanced extracellular glutamate levels in Cx30$^{-/-}$Cx43$^{-/-}$ mice, because their expression levels were unchanged (Fig. S6*A*), and the prolonged decay times of NMDAR EPSCs, reflecting glutamate spillover, occur although neuronal GLTs were inhibited by depolarization (at +50 mV) of the postsynaptic neuron (Fig. S6*B*). Altogether these findings indicate that disconnected astrocytes inadequately remove synaptically released glutamate, which accumulates and prolongs neuronal excitatory activity.

Similarly, we found that during comparable neuronal activity (0.1 ms pulse, 0.1 Hz, fiber volley Cx30$^{-/-}$Cx43$^{-/-}$, −0.15 ± 0.02 mV, $n = 5$ vs. WT, −0.18 ± 0.01 mV, $n = 5$), extracellular potassium concentrations ($[K^+]_o$) rose to ∼110% higher levels in Cx30$^{-/-}$Cx43$^{-/-}$ mice, monitored by the evoked astrocytic

NEUROSCIENCE

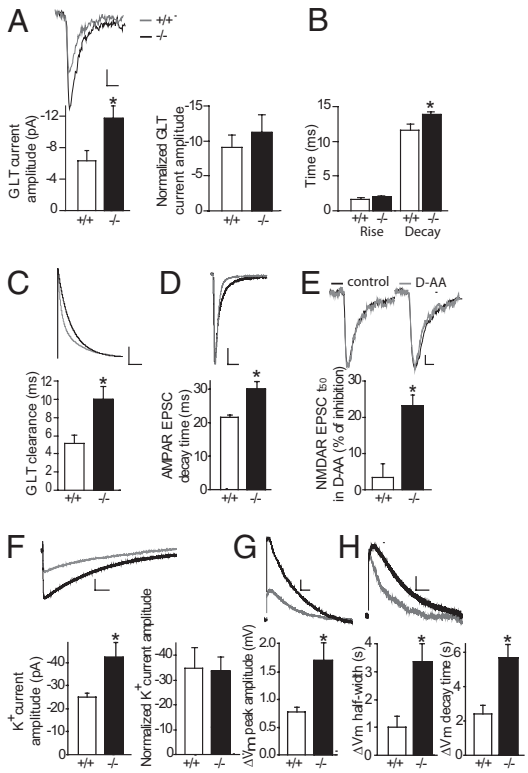

Fig. 4. Enhanced extracellular glutamate and potassium levels in Cx30$^{-/-}$Cx43$^{-/-}$ mice due to altered astroglial clearance. (*A*) Synaptically evoked astrocytic GLT currents are increased in Cx30$^{-/-}$Cx43$^{-/-}$ mice ($P < 0.05$, $n = 6$), compared with wild-type mice ($n = 6$). Normalization to the associated excitatory synaptic transmission (fEPSP slope/fiber volley ratio) reveals similar GLT current amplitudes. (Scale bar of representative current traces, 2.5 pA, 20 ms.) (*B*) GLT current decay time is prolonged in Cx30$^{-/-}$Cx43$^{-/-}$ astrocytes ($P < 0.05$, $n = 10$) compared with wild-type astrocytes ($n = 9$). (*C*) Deconvolution-derived astroglial glutamate clearance by GLTs is slower in Cx30$^{-/-}$Cx43$^{-/-}$ mice ($P < 0.05$, $n = 5$), compared with wild-type mice ($n = 5$). (*C*, *Upper*) Mean glutamate clearance time courses in wild-type and Cx30$^{-/-}$Cx43$^{-/-}$ mice, normalized and superimposed, are shown. (Scale bar, 0.2, 10 ms.) (*D*) Decay time of evoked AMPAR currents, recorded in the presence of cyclothiazide (100 μM), is increased in pyramidal cells from Cx30$^{-/-}$Cx43$^{-/-}$ mice ($P < 0.01$, $n = 5$, WT $n = 6$). (Scale bar, 20 pA, 50 ms.) (*E*) D-AA (70 μM) speeds the decay kinetics (t_{50}) of evoked NMDAR EPSCs (recorded at −70 mV in 10 μM CNQX), only in Cx30$^{-/-}$Cx43$^{-/-}$ mice ($P < 0.05$, $n = 5$; WT $n = 5$). (Scale bar of representative current traces, 10 pA, 50 ms.) (*F*) Synaptically evoked astrocytic potassium currents are increased in Cx30$^{-/-}$Cx43$^{-/-}$ mice ($P < 0.05$, $n = 8$; wild type mice, $n = 7$). Normalization to the associated excitatory synaptic transmission is shown. (Scale bar of representative current traces, 10 pA, 1 s.) (*G*) Extracellular potassium rise, evoked by comparable Schaffer collateral stimulation (0.1 ms, 0.1 Hz) and monitored by astroglial membrane potential depolarization (ΔV_m), is increased in Cx30$^{-/-}$Cx43$^{-/-}$ mice ($P < 0.05$, $n = 5$; wild-type mice, $n = 5$). (Scale bar, 0.2 mV, 1.5 s.) (*H*) Kinetics of similar ΔV_m amplitudes (Cx30$^{-/-}$Cx43$^{-/-}$, 1.1 ± 0.1 mV, $n = 5$ vs. WT, 0.9 ± 0.1 mV, $n = 5$) revealed increased half width ($P < 0.05$) and decay time ($P < 0.01$) in Cx30$^{-/-}$Cx43$^{-/-}$ astrocytes. (Scale bar, 0.2 mV, 2 s.)

membrane potential depolarization (17) (Fig. 4*G*). In addition, astrocyte uncoupling prolongs the removal of $[K^+]_o$, indicated by the approximately threefold increased decay time and half-width of synaptically evoked astroglial membrane potential depolarizations, measured for similar amplitude events in Cx30$^{-/-}$Cx43$^{-/-}$ and wild-type mice (Cx30$^{-/-}$Cx43$^{-/-}$, 1.1 ± 0.1 mV, $n = 5$ vs. WT, 0.9 ± 0.1 mV, $n = 5$; Fig. 4*H*). Therefore, potassium buffering by Cx30$^{-/-}$Cx43$^{-/-}$ astrocytes is insufficient to remove efficiently the higher $[K^+]_o$. However, in basal conditions, we found normal ambient extracellular potassium and glutamate levels in Cx30$^{-/-}$Cx43$^{-/-}$ mice, indicated by unchanged resting membrane potentials of CA1 pyramidal cells (V_m, Cx30$^{-/-}$Cx43$^{-/-}$, −59.7 ± 0.7 mV, $n = 38$ vs. WT, −59.5 ± 0.9 mV, $n = 34$) and astrocytes (Fig. S1*E*), as well as by similar tonic NMDAR currents (Fig. S4*B*), respectively.

Prominent cell swelling may also occur in Cx30$^{-/-}$Cx43$^{-/-}$ astrocytes, because they still take up high amounts of extracellular potassium and glutamate (Fig. 4 *A* and *F*), associated with water coentry to equilibrate intracellular osmolarity, and are unable to redistribute them via the network. Therefore, we analyzed astrocyte morphology in the *stratum radiatum* region and found that astrocytes labeled with sulforhodamine 101 were hypertrophic and displayed larger soma in Cx30$^{-/-}$Cx43$^{-/-}$ mice than in wild-type mice (Fig. 5*A*), as recently shown by electron microscopy in adult Cx30$^{-/-}$Cx43$^{-/-}$ mice (4). Furthermore, GFAP immunoreactivity was enhanced (Fig. 5*B*) and revealed that Cx30$^{-/-}$Cx43$^{-/-}$ astrocytes occupy larger domain areas (Cx30$^{-/-}$Cx43$^{-/-}$, 1900 ± 10 μm^2, $n = 31$ vs. WT, 1200 ± 5 μm^2, $n = 31$; Fig. 5*D*), associated with an elongation of their processes (Cx30$^{-/-}$Cx43$^{-/-}$, 36 ± 1 μm, $n = 54$ vs. WT, 28 ± 0.8 μm, $n = 54$; Fig. 5*E*). Because enhanced expression of GFAP and hypertrophy of astrocytes are hallmarks of reactive gliosis, we investigated whether astrocytes from Cx double-knockout mice were reactive by using the vimentin marker. Vimentin expression, absent in CA1 wild-type astrocytes, was detected in Cx30$^{-/-}$Cx43$^{-/-}$ astrocytes (Fig. 5*C*). To investigate whether increased size of astrocytic volume during synaptic activity affects extracellular space (ECS) volume, we measured the concentration of an extracellular marker, tetramethylammonium (TMA^+), by ion-selective microelectrodes (Fig. 6*A*). During Schaffer collateral stimulation (10 Hz/10 s), the relative decrease in ECS volume was doubled in Cx30$^{-/-}$Cx43$^{-/-}$ mice (Fig. 6 *B* and *C*), calculated by the increase in the extracellular concentration of TMA^+ from the baseline level in CA1 *stratum radiatum* ($P < 0.0001$, Cx30$^{-/-}$Cx43$^{-/-}$, 37.2 ± 1.9 μM, $n = 9$ vs. WT, 18 ± 0.9 μM, $n = 8$; Fig. 6*B*). Therefore, decreased ECS volume in Cx30$^{-/-}$Cx43$^{-/-}$ mice, by further increasing extracellular concentrations of ions and neurotransmitters, and possibly leading to an accumulation of diffusion barriers slowing down ECS diffusion, will enhance even more synaptic activity and prolong neuronal activation. In addition, the action of neuroactive substances in the ECS will be further prolonged by the delayed deswelling of Cx30$^{-/-}$Cx43$^{-/-}$ astrocytes following neuronal activity,

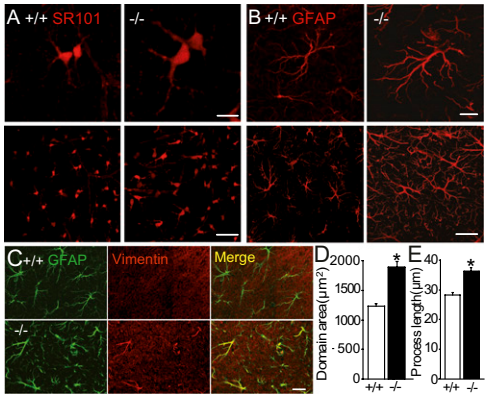

Fig. 5. Uncoupled astrocytes are hypertrophic and reactive. (*A*) Cx30 and -43 deficiency causes enhanced size of *stratum radiatum* astrocytes, as detected by sulforhodamine-101 (SR101) labeling (Cx30$^{-/-}$Cx43$^{-/-}$, $n = 3$; WT, $n = 3$). (Scale bars, 10 μm and 30 μm.) (*B*, *D*, and *E*) Increased GFAP immunoreactivity ($n = 3$, *B*) and enlarged domain areas of Cx30$^{-/-}$Cx43$^{-/-}$ astrocytes ($P < 0.0001$, $n = 31$; WT, $n = 33$, *D*), due to process elongation ($P < 0.0001$, Cx30$^{-/-}$Cx43$^{-/-}$, $n = 54$; WT, $n = 54$, *E*). (*C*) Astrocytes from Cx30$^{-/-}$Cx43$^{-/-}$ mice ($n = 3$) are reactive, as shown by vimentin immunoreactivity ($n = 3$). (Scale bar, 30 μm.)

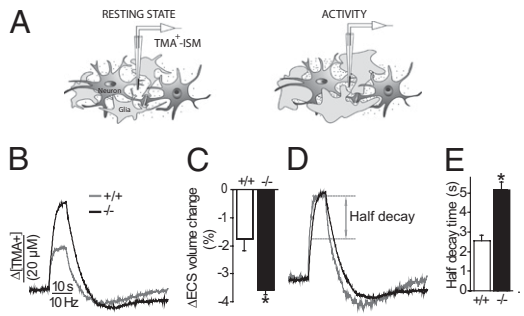

Fig. 6. Enhanced extracellular space volume reduction during neuronal activity in $Cx30^{-/-}Cx43^{-/-}$ mice. (*A*) Scheme illustrating the increase in extracellular concentration of TMA^+ ions during neuronal activity due to cell swelling. (*B*) Representative traces of the time-dependent concentration change of the extracellular marker tetramethyammonium (TMA^+) during 10 Hz/10 s Schaffer collateral stimulation, recorded in the *stratum radiatum* of the CA1 region. (*C*) Calculated relative changes in the extracellular space (ECS) volume ($Cx43^{-/-}Cx30^{-/-}$, $n = 9$; WT, $n = 8$). (*D* and *E*) Normalized representative TMA^+ responses (*D*) show increased half-decay time (*E*) ($P < 0.0001$, $Cx30^{-/-}Cx43^{-/-}$, $n = 9$; WT, $n = 8$).

indicated by the ~100% increase in half decay time of the normalized TMA^+ responses (Fig. 6 *D* and *E*).

Discussion

Our findings establish astroglial gap junction-mediated networks as major determinants of extracellular homeostasis, which control functions of the pre- and postsynaptic elements, as well as their associated bidirectional synaptic plasticity. Indeed, connexin-mediated astroglial networks scale synaptic activity, as they define the concentrations and dynamics of extracellular ions and neurotransmitters during synaptic activity. Although disconnected astrocytes still manage to take up high levels of released potassium and glutamate during synaptic activity, they are unable to redistribute them via the network; swell due to intracellular accumulation of high amounts of potassium, glutamate, and cotransported water; and fail to remove the neuroactive substances efficiently, as shown by the reduced astroglial glutamate clearance through GLTs, prolonged decay times of neuronal AMPA and NMDA currents, and astroglial membrane depolarizations. Because astrocyte depolarization and ion gradient disturbances inhibit GLT activity (18–23), the decreased glutamate clearance by $Cx30^{-/-}Cx43^{-/-}$ astrocytes may also result from the prolonged astroglial depolarization and enhanced $[K^+]_o$ we found during synaptic activity. Furthermore, because astrocytes occupy 50% of the brain volume (24), their swelling decreases significantly ECS volume during neuronal activity and thereby can also contribute to the strong and prolonged increase in the extracellular concentrations of ions and neurotransmitters (25). These data reveal a major role for astrocytic networks in glutamate clearance, potassium buffering, and ECS volume regulation during basal synaptic activity. Indeed until now, a contribution of astroglial networks to glutamate clearance was not shown, although glutamate, once taken up by astrocytes, can diffuse and be dissipated through gap junction channels in astrocytic networks (26), and a role for potassium buffering was assessed only during trains of high stimulation and epileptiform activity in the absence of postsynaptic activity (6), which nevertheless represents the main source (80%) of extracellular potassium accumulation (27). In addition, astrocytes are well known to contact postsynaptic elements (24) and therefore influence $[K^+]_o$ at these microcompartments, as we found during intact pre- and postsynaptic activities.

Disruption of astrocytic networks has a major impact on neurotransmission, due to combined pre- and postsynaptic alterations, including enhanced neuronal excitability, release probability, and insertion of postsynaptic AMPARs, unsilencing synapses. Our findings point to a direct contribution of connexin-mediated astroglial networks to ongoing synaptic transmission, because altered physiology of $Cx30^{-/-}Cx43^{-/-}$ astrocytes leading to increased extracellular potassium and glutamate levels occurs only during evoked basal synaptic activity. Furthermore, it seems unlikely that alterations of neuronal activity are due to major developmental defects in $Cx30^{-/-}Cx43^{-/-}$ mice, because we found no change in the architecture of the hippocampus, presenting normal layered structure; in the numbers of hippocampal CA1 astrocytes and neurons, as already reported (4); in the levels of the pre- and postsynaptic proteins synaptophysin and PSD-95, respectively, suggesting similar total synaptic contacts; and in the number of synaptic inputs received by CA1 pyramidal cells, as assessed by similar size of the NMDA current induced by minimal stimulation in $Cx30^{-/-}Cx43^{-/-}$ and wild-type mice. Furthermore, LTP could be restored in $Cx30^{-/-}Cx43^{-/-}$ mice by synapse depotentiation, indicating that the underlying neuronal functionality is preserved.

Enhanced release probability from CA3 inputs may reflect increased extracellular potassium and glutamate levels evoked by synaptic stimulation (28, 29) resulting from decreased astroglial clearance and ECS, as well as the likely slower extracellular diffusion due to astroglial volume increase (25). Furthermore in CA1 pyramidal cells, the enhancement in synaptic activity is not specific for excitatory transmission, but also affects inhibitory inputs. This result strongly suggests that ECS volume reduction concentrates various neuroactive substances, such as glutamate, potassium, and GABA. Surprisingly, CA1 pyramidal cells have also increased postsynaptic AMPAR density in $Cx43^{-/-}Cx30^{-/-}$ mice. Although homeostatic synaptic scaling, adjusting synaptic strength to compensate for changes in activity (30), should induce a decrease in postsynaptic AMPAR density in $Cx43^{-/-}Cx30^{-/-}$ mice, our data suggest that persistent elevated glutamatergic input over development increased recruitment of synaptic AMPARs, known to be activity dependent (8). Interestingly, we found that disruption of astrocytic networks has no impact on the total number of synapses, but converts silent synapses to functional ones at CA1 pyramidal cells, indicating that enhanced recruitment of functional AMPARs unsilences synapses during development (8). This regulation has important consequences for synaptic plasticity as conversion of silent synapses to functional synapses at CA1 pyramidal cells occurs during LTP (8). Indeed, we found that astroglial networks are crucial for synaptic plasticity, because the reduced pool of silent synapses in $Cx30^{-/-}Cx43^{-/-}$ mice occluded LTP and increased the magnitude of LTD. Therefore, unsilencing synapses in $Cx30^{-/-}Cx43^{-/-}$ mice strongly shifts the threshold balance between LTP and LTD, the cellular substrates for learning and memory, favoring synaptic depression. Such a shift in LTP and LTD balance was also found in other studies, where postsynaptic AMPAR density was increased by overexpressing PSD-95, resulting in less silent synapses (31–33). Because synapse depotentiation restored LTP, this result further confirms that the defect in LTP in $Cx30^{-/-}Cx43^{-/-}$ mice is downstream of NMDAR activation.

The significance of astroglial networks for normal brain functions is highlighted by impairments in sensorimotor and spatial memory tasks in $Cx43^{-/-}Cx30^{-/-}$ mice (4). Therefore, during physiological conditions, astroglial network communication is crucial for precise synaptic information transfer, processing, and storage, because we show that it limits neuronal excitability, release probability, spillover, the number of functional synapses, and it controls short and long-term synaptic plasticity. Among the various substances crossing astrocyte gap junction channels, neurotransmitters and ions predominate to regulate basal synaptic activity. Indeed, although astroglial networks have recently been shown to sustain synaptic transmission by providing energy metabolites to distal neurons (5), such function is likely to be

NEUROSCIENCE

important in pathological conditions, such as hypoglycemia, altering energy production, or epilepsy, associated to neuronal hyperactivity. Dysfunction of astroglial networks over time should result in combined chronic increases in pre- and postsynaptic functions, leading to a vicious circle: higher neuronal activity causes more release, enhancing astroglial uptake (but insufficiently to remove efficiently the increased levels of neuroactive substances), resulting in swelling, reducing extracellular space volume, and increasing even more ion and neurotransmitter extracellular concentrations. This insidious process can abolish synapse independence, altering local information processing, and leads to a higher susceptibility to hypersynchronization, a hallmark of epilepsy (6), and to excitotoxicity at later developmental stages (4).

Methods

Experiments were carried out according to the guidelines of the European Community Council Directives of November 24, 1986 (86/609/EEC). Experiments were performed on the hippocampus of wild-type mice and Cx30$^{-/-}$Cx43fl/fl:hGFAP-Cre mice (Cx30$^{-/-}$Cx43$^{-/-}$, double knockout) (provided by K. Willecke, University of Bonn, Bonn, Germany), with conditional deletion of Cx43 in astrocytes (3) and additional total deletion of Cx30 (34), as previously described (6). For all analyses, mice of both genders and littermates were used (P16–P25). Detailed protocols for electrophysiology, biochemistry, and extracellular volume measurements are provided in *SI Methods*.

ACKNOWLEDGMENTS. We thank O. Chever, A. Tzingounis, D. Schmitz, and A. Koulakoff for helpful discussions and/or technical assistance, as well as K. Willecke for providing the Cx30$^{-/-}$Cx43fl/fl:hGFAP-Cre mice. This work was supported by grants from the Human Frontier Science Program Organization (Career Development Award), Agence Nationale de la Recherche (Programme Jeunes Chercheurs), and Institut National de la Santé et de la Recherche Médicale (to N.R.); postdoctoral fellowships from the French Research Ministry and Deutsche Forschungsgemeinschaft (to U.P.); and a grant from the Franco Czech Barrande Program (Hubert Curien Program) (to N.R. and L.V.), Grant 309/09/1597 from the Grant Agency of the Czech Republic (to L.V. and E.S.), Grant AVOZ50390512 from the Academy of Sciences of the Czech Republic (to E.S.) and Grant 1M0538 from the Ministry of Education, Youth and Sports of the Czech Republic (to E.S.).

1. Perea G, Navarrete M, Araque A (2009) Tripartite synapses: Astrocytes process and control synaptic information. *Trends Neurosci* 32:421–431.
2. Giaume C, Koulakoff A, Roux L, Holcman D, Rouach N (2010) Astroglial networks: A step further in neuroglial and gliovascular interactions. *Nat Rev Neurosci* 11:87–99.
3. Theis M, et al. (2003) Accelerated hippocampal spreading depression and enhanced locomotory activity in mice with astrocyte-directed inactivation of connexin43. *J Neurosci* 23:766–776.
4. Lutz SE, et al. (2009) Deletion of astrocyte connexins 43 and 30 leads to a dysmyelinating phenotype and hippocampal CA1 vacuolation. *J Neurosci* 29: 7743–7752.
5. Rouach N, Koulakoff A, Abudara V, Willecke K, Giaume C (2008) Astroglial metabolic networks sustain hippocampal synaptic transmission. *Science* 322:1551–1555.
6. Wallraff A, et al. (2006) The impact of astrocytic gap junctional coupling on potassium buffering in the hippocampus. *J Neurosci* 26:5438–5447.
7. Kunze A, et al. (2009) Connexin expression by radial glia-like cells is required for neurogenesis in the adult dentate gyrus. *Proc Natl Acad Sci USA* 106:11336–11341.
8. Kerchner GA, Nicoll RA (2008) Silent synapses and the emergence of a postsynaptic mechanism for LTP. *Nat Rev Neurosci* 9:813–825.
9. Isaac JT, Nicoll RA, Malenka RC (1995) Evidence for silent synapses: Implications for the expression of LTP. *Neuron* 15:427–434.
10. Diamond JS (2005) Deriving the glutamate clearance time course from transporter currents in CA1 hippocampal astrocytes: Transmitter uptake gets faster during development. *J Neurosci* 25:2906–2916.
11. Iino M, et al. (2001) Glia-synapse interaction through Ca2+-permeable AMPA receptors in Bergmann glia. *Science* 292:926–929.
12. Mennerick S, Zorumski CF (1994) Glial contributions to excitatory neurotransmission in cultured hippocampal cells. *Nature* 368:59–62.
13. Tsukada S, Iino M, Takayasu Y, Shimamoto K, Ozawa S (2005) Effects of a novel glutamate transporter blocker, (2S, 3S)-3-[3-[4-(trifluoromethyl)benzoylamino]benzyloxy]aspartate (TFB-TBOA), on activities of hippocampal neurons. *Neuropharmacology* 48:479–491.
14. Asztely F, Erdemli G, Kullmann DM (1997) Extrasynaptic glutamate spillover in the hippocampus: Dependence on temperature and the role of active glutamate uptake. *Neuron* 18:281–293.
15. Diamond JS (2001) Neuronal glutamate transporters limit activation of NMDA receptors by neurotransmitter spillover on CA1 pyramidal cells. *J Neurosci* 21: 8328–8338.
16. Levenson J, et al. (2002) Long-term potentiation and contextual fear conditioning increase neuronal glutamate uptake. *Nat Neurosci* 5:155–161.
17. Amzica F, Massimini M, Manfridi A (2002) Spatial buffering during slow and paroxysmal sleep oscillations in cortical networks of glial cells in vivo. *J Neurosci* 22: 1042–1053.
18. Bordey A, Sontheimer H (2003) Modulation of glutamatergic transmission by Bergmann glial cells in rat cerebellum in situ. *J Neurophysiol* 89:979–988.
19. D'Ambrosio R (2004) The role of glial membrane ion channels in seizures and epileptogenesis. *Pharmacol Ther* 103:95–108.
20. Djukic B, Casper KB, Philpot BD, Chin LS, McCarthy KD (2007) Conditional knock-out of Kir4.1 leads to glial membrane depolarization, inhibition of potassium and glutamate uptake, and enhanced short-term synaptic potentiation. *J Neurosci* 27: 11354–11365.
21. Mennerick S, et al. (1999) Substrate turnover by transporters curtails synaptic glutamate transients. *J Neurosci* 19:9242–9251.
22. Mennerick S, Zorumski CF (1995) Presynaptic influence on the time course of fast excitatory synaptic currents in cultured hippocampal cells. *J Neurosci* 15:3178–3192.
23. Otis TS, Kavanaugh MP (2000) Isolation of current components and partial reaction cycles in the glial glutamate transporter EAAT2. *J Neurosci* 20:2749–2757.
24. Ventura R, Harris KM (1999) Three-dimensional relationships between hippocampal synapses and astrocytes. *J Neurosci* 19:6897–6906.
25. Syková E, Vargová L, Prokopová S, Simonová Z (1999) Glial swelling and astrogliosis produce diffusion barriers in the rat spinal cord. *Glia* 25:56–70.
26. Giaume C, Tabernero A, Medina JM (1997) Metabolic trafficking through astrocytic gap junctions. *Glia* 21:114–123.
27. Poolos NP, Mauk MD, Kocsis JD (1987) Activity-evoked increases in extracellular potassium modulate presynaptic excitability in the CA1 region of the hippocampus. *J Neurophysiol* 58:404–416.
28. Hablitz JJ, Lundervold A (1981) Hippocampal excitability and changes in extracellular potassium. *Exp Neurol* 71:410–420.
29. Raffaelli G, Saviane C, Mohajerani MH, Pedarzani P, Cherubini E (2004) BK potassium channels control transmitter release at CA3-CA3 synapses in the rat hippocampus. *J Physiol* 557:147–157.
30. Turrigiano GG (2008) The self-tuning neuron: Synaptic scaling of excitatory synapses. *Cell* 135:422–435.
31. Béïque JC, Andrade R (2003) PSD-95 regulates synaptic transmission and plasticity in rat cerebral cortex. *J Physiol* 546:859–867.
32. Ehrlich I, Malinow R (2004) Postsynaptic density 95 controls AMPA receptor incorporation during long-term potentiation and experience-driven synaptic plasticity. *J Neurosci* 24:916–927.
33. Stein V, House DR, Bredt DS, Nicoll RA (2003) Postsynaptic density-95 mimics and occludes hippocampal long-term potentiation and enhances long-term depression. *J Neurosci* 23:5503–5506.
34. Teubner B, et al. (2003) Connexin30 (Gjb6)-deficiency causes severe hearing impairment and lack of endocochlear potential. *Hum Mol Genet* 12:13–21.